J. Iron Steel Res. Int. (2020) 27:913–921
https://doi.org/10.1007/s42243-020-00444-7

ORIGINAL PAPER

Influence of refining process and utilization of different slags on inclusions, titanium yield and total oxygen content of Ti-stabilized 321 stainless steel

Xing-run Chen[1,2] · Guo-guang Cheng[1] · Yu-yang Hou[1] · Jing-yu Li[1] · Ji-xiang Pan[2]

Received: 22 May 2019 / Revised: 22 November 2019 / Accepted: 22 November 2019 / Published online: 25 June 2020

Abstract
Ti-stabilized 321 stainless steel was prepared using an electric arc furnace, argon oxygen decarburization (AOD) furnace, ladle furnace (LF), and continuous casting processes. In addition, the effect of refining process and utilization of different slags on the evolution of inclusions, titanium yield, and oxygen content was systematically investigated by experimental and thermodynamic analysis. The results reveal that the total oxygen content (TO) and inclusion density decreased during the refining process. The spherical CaO–SiO_2–Al_2O_3–MgO inclusions existed in the 321 stainless steel after the AOD process. Moreover, prior to the Ti addition, the spherical CaO–Al_2O_3–MgO–SiO_2 inclusions were observed during LF refining process. However, Ti addition resulted in multilayer CaO–Al_2O_3–MgO–TiO_x inclusions. Two different samples were prepared by conventional CaO–Al_2O_3-based slag (Heat-1) and TiO_2-rich CaO–Al_2O_3-based slag (Heat-2). The statistical analysis revealed that the density of inclusions and the TiO_x content in CaO–Al_2O_3–MgO–TiO_x inclusions found in Heat-2 sample are much lower than those in the Heat-1 sample. Furthermore, the TO content and Ti yield during the LF refining process were controlled by using TiO_2-rich calcium aluminate synthetic slag. These results were consistent with the ion–molecule coexistence theory and FactSage™7.2 software calculations. When TiO_2-rich CaO–Al_2O_3-based slag was used, the TiO_2 activity of the slag increased, and the equilibrium oxygen content significantly decreased from the AOD to LF processes. Therefore, the higher TiO_2 activity of slag and lower equilibrium oxygen content suppressed the undesirable reactions between Ti and O.

Keywords 321 Austenitic stainless steel · Oxygen content · Inclusion · TiO_2-rich CaO–Al_2O_3-based slag · Ladle furnace (LF) refining process · Ion–molecule coexistence theory

1 Introduction

As a Ti-stabilized austenitic stainless steel (SS), 321 SS renders a set of unique advantages, such as superior high-temperature strength, adequate creep resistance, and excellent oxidation and corrosion resistance, compared to 304 stainless steel. Hence, 321 SS is widely used in heat exchangers, high-pressure pipes, engine turbines, aerospace exhaust manifolds, and nuclear industry [1–5]. Nevertheless, as a Ti-stabilized steel, 321 steel has several casting and operational challenges such as low Ti yield, submerged entry nozzle (SEN) clogging during casting, deterioration of mold flux, defects on slab surface and line defects, which are quite similar to the issue with other Ti-stabilized stainless steels [6–11].

Therefore, different research groups aimed to understand and use various strategies to resolve these issues. For instance, Yin et al. [12] reported the formation of inclusions in Ti-stabilized 17Cr austenitic SS. The results revealed that tapping and Ti wire feeding result in pure TiN particles and complex TiN-containing inclusions, with Al_2O_3–MgO–TiO_x core, at a Ti content of 0.307 wt.%. Qian et al. [13] reported that the oxidation rate of Ti initially decreased with increasing TiO_2 content in slag and reached a minimum level at TiO_2 content of 8 wt.% in the slag, followed by a gradual increase. Kang et al. [14, 15] pointed out that Rb_2O and Cs_2O allow significant removal of TiN inclusions because of the ion compensation effect and supplementary free

✉ Guo-guang Cheng
chengguoguang@metall.ustb.edu.cn

1 State Key Laboratory of Advanced Metallurgy, University of Science and Technology Beijing, Beijing 100083, China

2 Hongxing Iron and Steel Co., Ltd., Jiuquan Iron and Steel Group Corporation, Jiayuguan 735100, Gansu, China

oxygen ions, whereas at the same time, the viscosity of the slag increased to retain the absorbed inclusions. Moreover, compared to the preexisting tundish flux compositions, K_2O incorporation significantly improved the cleanliness of the as-quenched 321 stainless steel melts. Zheng and Chen [16] found the optimal composition for the formation of $CaO–TiO_2–MgO–Al_2O_3$ in 321 SS, exhibiting that the concentration of Ca, Ti, and Al should be higher than 0.001, 0.1, and 0.01 wt.%, respectively. Seo et al. [17] demonstrated that the Al deoxidation/Ca treatment/Ti alloying pattern of the ladle refining operation effectively reduces the spinel formation in Ti-stabilized steels and extends the life cycle of SEN nozzle. Lencina et al. [18] described the positive effect of TiO_2-rich calcium aluminate flux in the formation of slags for 321 stainless steel. While previous reports have described the inclusions evolution of 321 stainless steel and some strategies to improve the cleanliness of the molten steel, the effect of different refining slags on the titanium yield, oxygen content, and inclusions during ladle furnace refining process has not yet been studied.

In this study, the titanium yield, the inclusions evolution, and oxygen content variation in 321 austenitic stainless steel under different refining slag conditions, produced by electric arc furnace (EAF), argon oxygen decarburization furnace (AOD), ladle furnace (LF), and continuous casting (CC) processes were systematically investigated. The role of TiO_2-rich calcium aluminate synthetic slag on inclusions, titanium yield, and oxygen content was investigated by experimental analysis and thermodynamic calculations.

2 Experimental

2.1 Steel fabrication and sampling

The 321 stainless steel was prepared by EAF-AOD-LF-CC process. First, the ferronickel, ferrochromium, and steel scrap were melted in an EAF, and subsequently the molten steel was poured into an AOD. After decarburization in the AOD, the chromium oxide was reduced by adding ferrosilicon. Once the reduction was completed, the desulfurization process was conducted to obtain the target value of binary basicity ($w_{CaO}/w_{SiO_2} = 2.50$). Figure 1 shows an illustration of the operation and sampling processes during the refining stage, where the time at which AOD was finished was assumed as 0 min. The slag was tapped after the AOD process, and the ladle was hanged to the LF. Magnesia–calcium was used as the refractory material. The aluminum wires were fed into the molten steel to achieve the target value of 0.03 wt.%, followed by calcium treatment. Next, the refining slag was added for secondary refining, followed by titanium-alloying operation. Finally, the liquid steel was transported to the platform for continuous casting at the designated temperature and composition values. The industrial experiments involved different refining slags. For instance, Heat-1 used normal $CaO–Al_2O_3$ based slag, and Heat-2 utilized TiO_2-rich calcium aluminate slag. The steel samples were taken after the AOD treatment, before titanium-alloying operation and after titanium-alloying operation during the LF refining process to analyze the steel composition and level of inclusions. Moreover, the slag samples were taken at the same time. Sample-A was collected after the AOD treatment, whereas LF1 and LF2 were collected before and after titanium-alloying operation during the LF refining process, respectively.

2.2 Characterization

The chemical composition of the steel samples (ϕ30 mm × 10 mm) was determined by a direct reading spectrum. The C and S contents were analyzed using a C/S analyzer (CS-800, ELTRA, Haan, Germany). The cylindrical samples (ϕ5 mm × 5 mm) were machined to measure the total oxygen content using an O/N analyzer (EMGA-620 W, Horiba, Kyoto, Japan). The composition of the slags was analyzed by X-ray fluorescence spectrometry (ARL PERFORM'X, Thermo Fisher Scientific, MA, USA).

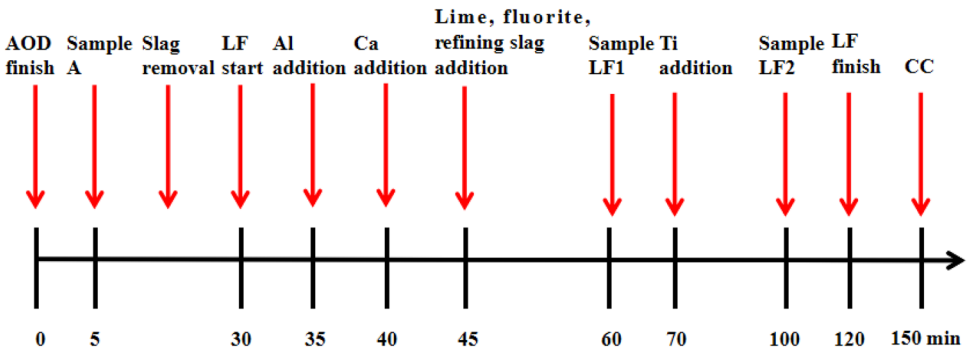

Fig. 1 Illustration of operation and sampling processes during refining process

Table 1 Chemical composition of 321 stainless steel at different stages (wt.%)

Heat	Stage	C	Si	Mn	P	S	Ni	Cr	Al	Ti	N
Heat-1	A	0.015	0.438	1.213	0.022	0.001	9.029	17.273	0.009	0.003	0.009
	LF1	0.020	0.568	1.234	0.022	0.001	9.136	17.334	0.028	0.004	0.012
	LF2	0.026	0.593	1.221	0.022	0.001	9.104	17.197	0.024	0.291	0.012
Heat-2	A	0.014	0.491	1.234	0.028	0.001	9.019	17.300	0.009	0.002	0.007
	LF1	0.021	0.584	1.234	0.028	0.001	9.182	17.299	0.027	0.009	0.010
	LF2	0.027	0.605	1.218	0.028	0.001	9.210	17.278	0.026	0.272	0.011

Table 2 Chemical composition of slag at different stages (wt.%)

Heat	Stage	CaO	CaF_2	MgO	Al_2O_3	SiO_2	TiO_2	TFe	MnO	Cr_2O_3	S
Heat-1	A	57.67	9.38	2.67	6.40	22.45	0.30	0.40	0.06	0.50	0.17
	LF1	55.81	7.41	3.35	15.94	16.73	0.35	0.12	0.05	0.15	0.09
	LF2	55.64	6.98	3.46	14.87	16.07	2.49	0.15	0.03	0.21	0.10
Heat-2	A	52.40	12.67	2.86	6.33	18.56	0.26	3.05	0.16	3.39	0.32
	LF1	60.87	6.86	3.45	17.45	7.95	3.05	0.15	0.05	0.10	0.07
	LF2	59.99	6.39	4.57	16.92	8.41	3.29	0.17	0.04	0.15	0.07

Moreover, steel samples (10 mm × 10 mm × 10 mm) were machined to analyze the morphology and composition of the inclusions. The surface was ground by using SiC paper (1200 grit), followed by polishing with diamond paste. The chemical composition of the inclusions was determined by energy-dispersive spectroscopy (EDS, X-Max 80, Oxford Instruments, High Wycombe, UK) coupled to scanning electron microscopy (SEM, Merlin Compact, Zeiss, Gottingen, Germany). For each sample, ~30 inclusions were selected for characterization. In addition, quantitative analysis of inclusions size was performed by using INCA software (Inca Energy 250, Oxford Instruments, High Wycombe, UK) of the scanning electron microscope. A sample size larger than 1 μm was used to enhance the accuracy of EDS analysis of the inclusions. The scanning area was 5.48×10^7 μm^2.

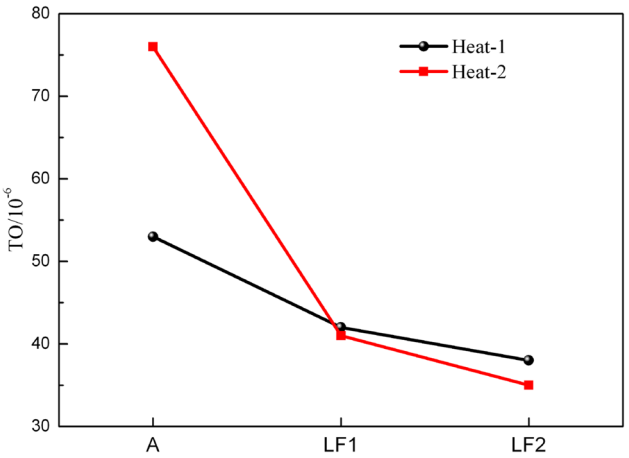

Fig. 2 Total oxygen content in 321 stainless steel at different stages of steelmaking process

3 Results

3.1 Composition of molten steel and slag

The composition of different steels and slags is listed in Tables 1 and 2, respectively. Heat-1 utilized normal CaO-Al_2O_3-based slag and both (CaO/SiO_2) and Al_2O_3 contents in the slag increased from A to LF1, whereas the SiO_2 content decreased. After feeding Ti wire in the LF process, the TiO_2 content increased from 0.35 to 2.49 wt.%, showing the oxidation of Ti in the slag. In contrast, Heat-2 utilized TiO_2-rich calcium aluminate slag. Hence, both (CaO/SiO_2) and Al_2O_3 content in the slag increased from A to LF1, whereas compared to Heat-1, the total iron (TFe), MnO, and Cr_2O_3 contents significantly decreased. The amount of TiO_2 in slag increased with the addition of Ti into molten steel; however, the variation is extremely negligible.

3.2 Oxygen content in 321 stainless steel

Figure 2 shows the TO evolution for Heat-1 and Heat-2 samples at different stages, indicating that the total oxygen content in both samples decreased during the steelmaking process. The total oxygen content in Heat-1 and Heat-2 after the AOD process was 53×10^{-6} and 76×10^{-6}, respectively. However, the total oxygen content in the molten steel

effectively reduced after secondary refining. The total oxygen content of Heat-2 decreased by 35×10^{-6}, which is three times as much as that of the Heat-1, prepared using normal $CaO–Al_2O_3$-based slag. During the refining process, the inclusions in molten steel constantly floated into the slag under argon stirring. Since these small inclusions grew, floated, and adsorbed by the slag after collision with each other, the total oxygen content of Heat-1 and Heat-2 samples decreased to 38×10^{-6} and 35×10^{-6}, respectively.

3.3 Titanium yield during LF refining process

Figure 3 shows the Ti yield of Heat-1 and Heat-2 samples during the refining process, indicating that Heat-2 samples exhibited higher Ti yield than Heat-1 samples, and this can be ascribed to the utilization of TiO_2-rich $CaO–Al_2O_3$-based slag instead of normal $CaO–Al_2O_3$-based slag. In general, the recovery of Heat-2 was improved by 9.0%.

3.4 Inclusion types at different stages

The morphology and composition of the inclusions in molten steel during the refining process were characterized, as shown in Fig. 4. The elemental mapping of the typical inclusions in molten steel is shown in Fig. 5, clearly indicating that the spherical $CaO–SiO_2–Al_2O_3–MgO$ inclusions, ranging from several to tens of microns, exist in 321 stainless steel after the AOD process. Moreover, these inclusions contain a small amount of magnesium and aluminum. The composition of the inclusions after the AOD (size larger than 10 μm) was almost the same as the slag composition. The $CaO–SiO_2–Al_2O_3–MgO$ inclusions which are smaller than 10 μm mainly originated from the oxidation reaction with Ca, Al, Mg, and Si. The Ca mainly derived from the metal-slag reaction and the metal-refractory reaction. The Mg content in the steel originated from slag and refractory material.

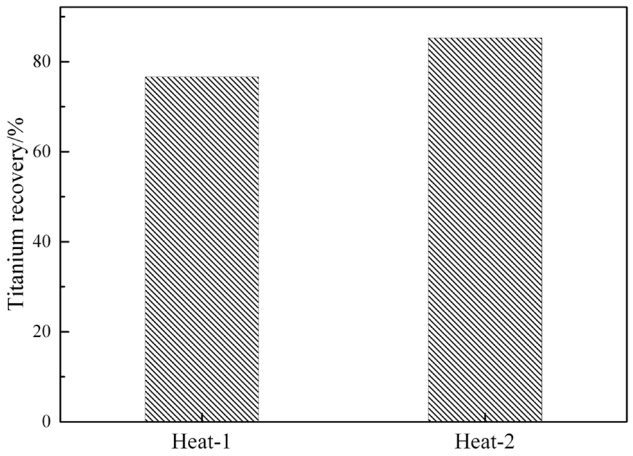

Fig. 3 Ti yield of Heat-1 and Heat-2 samples during refining process

Hence, the inclusion type was $CaO–Al_2O_3–MgO–SiO_2$ spherical inclusion before titanium-alloying operation during the LF process. In addition, the Al_2O_3 content of these inclusions was higher than that of the AOD process, whereas some parts of inclusions exhibited Mg-rich regions. However, the inclusions changed to multilayer $CaO–Al_2O_3–MgO–TiO_x$ inclusions after the titanium addition, as shown in Fig. 4c, f, where the black-colored areas correspond to higher Al_2O_3 and MgO contents, whereas the gray-colored regions represent $CaO–Al_2O_3–TiO_x$. Notably, MgO has been non-uniformly distributed, where a few inclusions exhibited lower content of MgO and others showed MgO enrichment in the local regions. In general, the TiO_x content of inclusions in Heat-2 samples was lower than that of Heat-1 samples.

3.5 Composition of inclusions at different stages

To elucidate the evolution of inclusions at different stages, the inclusions were plotted on the ternary phase diagram, as shown in Fig. 6. After the AOD process, the inclusions were almost the same as for Heat-1 and Heat-2 samples. Before the Ti addition during the LF refining process, the total Al_2O_3 and MgO content of inclusions significantly increased; however, the $CaO–Al_2O_3–MgO–SiO_2$ inclusions transformed into $CaO–Al_2O_3–MgO–TiO_x$ inclusions after the Ti addition. Moreover, the TiO_x content in Heat-2 sample was lower than that of Heat-1 sample.

3.6 Inclusion size and number density at different stages

The size distribution of inclusions, at different stages of the steelmaking process, of both Heat-1 and Heat-2 samples is presented in Fig. 7. Both samples exhibited a dominant proportion of small-size inclusions ($\leq$ 10 μm); however, the concentration of large-size inclusions ($\geq$ 10 μm) decreased from A to LF2. After the Ti addition, the number density of small-size inclusions ($\leq$ 5 μm) significantly increased in both samples, and this phenomenon can be ascribed to the formation of the new inclusions. Overall, the concentration of inclusions in Heat-1 sample is lower than the Heat-2 sample after the AOD process. Before the Ti addition during the LF refining process, the inclusion concentration in Heat-2 samples significantly decreased compared to that in the LF1 stage of Heat-1 sample.

4 Discussion

The formation mechanism of inclusions during 321 stainless steel refining process is schematically illustrated in Fig. 8. The spherical $CaO–SiO_2–Al_2O_3–MgO$ inclusions

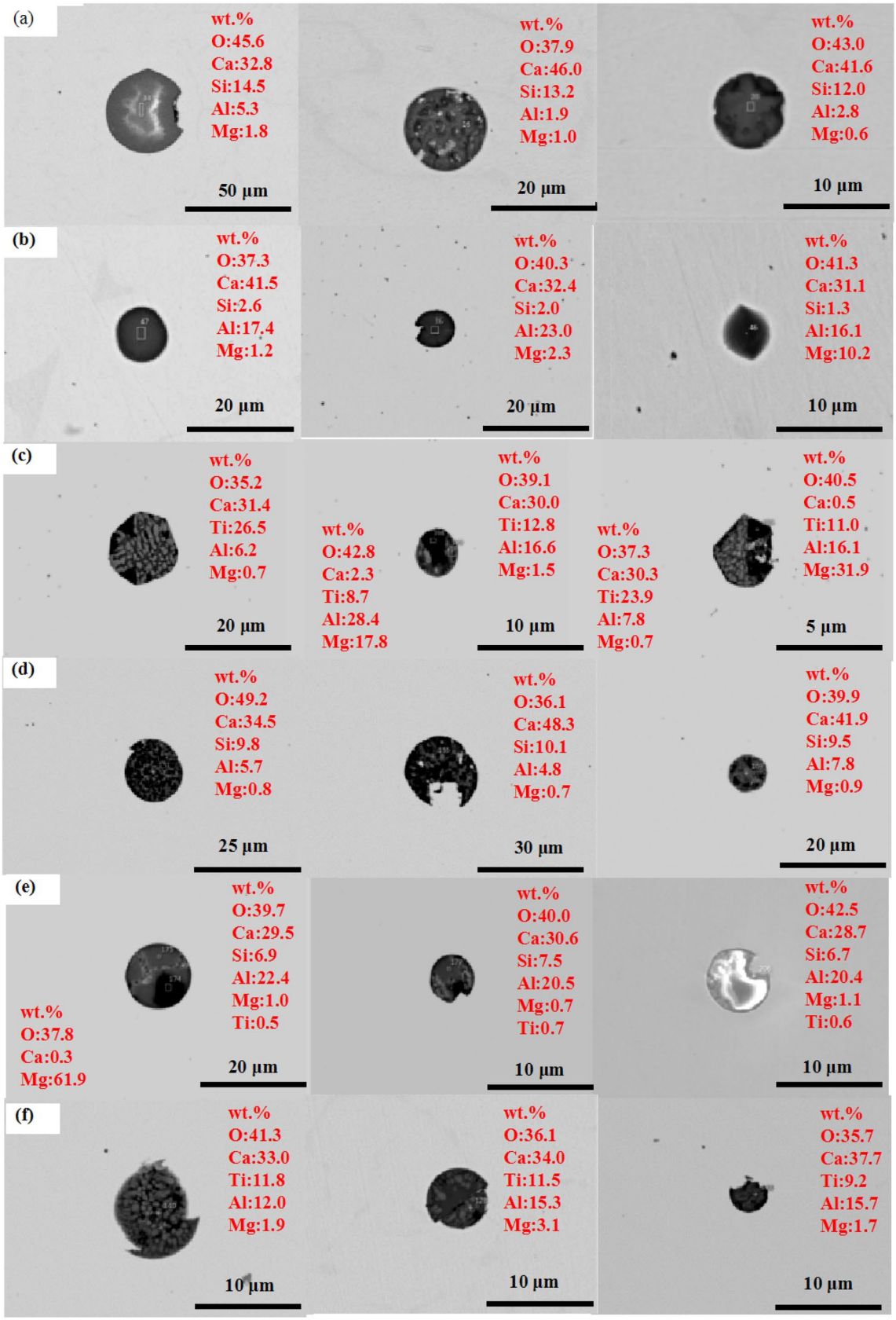

Fig. 4 Morphology and composition of typically encountered inclusions in Heat-1 and Heat-2 samples after various stages of steelmaking process. **a** Heat-1-A; **b** Heat-1-LF1; **c** Heat-1-LF2; **d** Heat-2-A; **e** Heat-2-LF1; **f** Heat-2-LF2

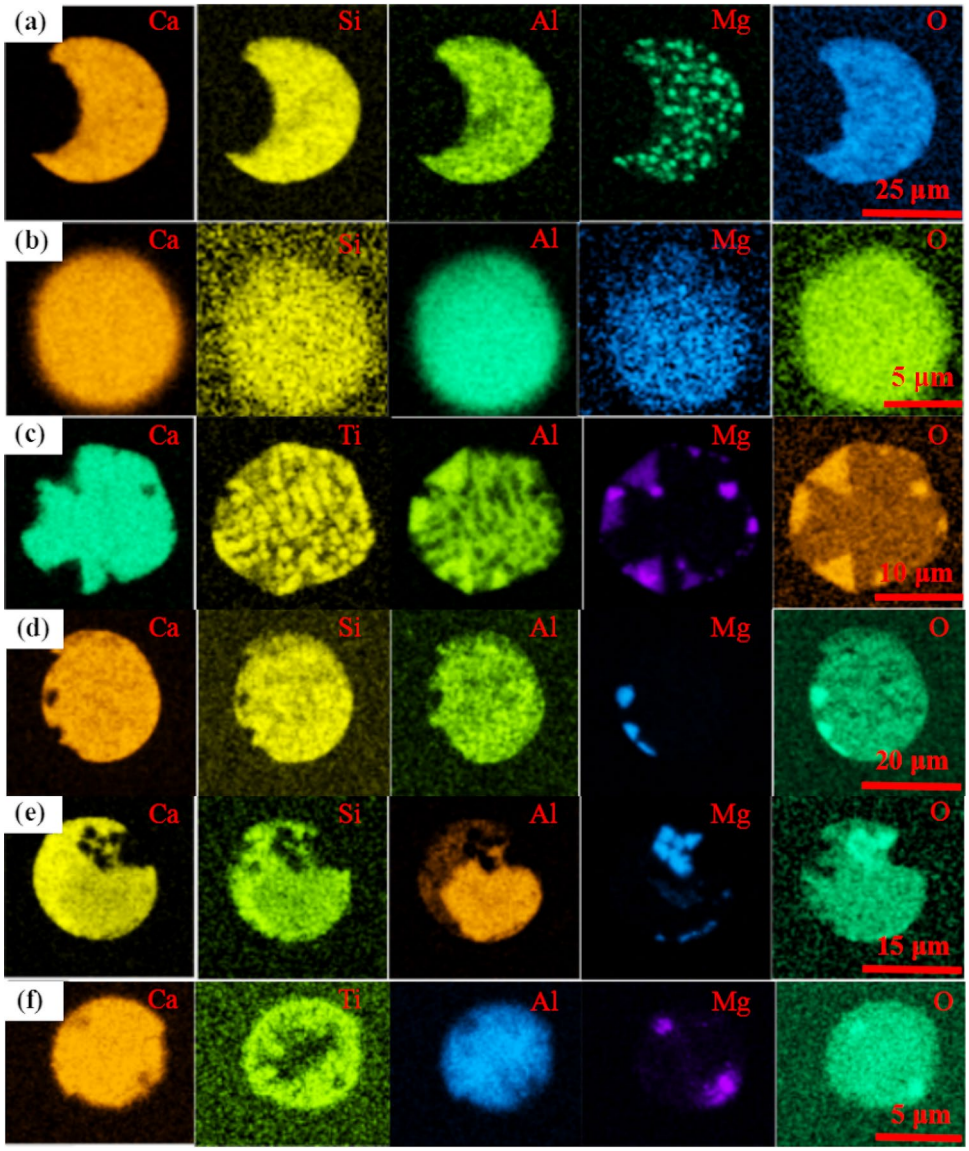

Fig. 5 Elemental maps of typically encountered inclusions in Heat-1 and Heat-2 samples. **a** Heat-1-A; **b** Heat-1-LF1; **c** Heat-1-LF2; **d** Heat-2-A; **e** Heat-2-LF1; **f** Heat-2-LF2

exist in 321 stainless steel after the AOD process. Then, Ca treatment was carried out after the Al addition for deoxidation, resulting in spherical $CaO–Al_2O_3–MgO–SiO_2$ inclusions. Once lime, fluorite, and $CaO–Al_2O_3$-based refining slag were added for secondary refining, large-size inclusions (> 10 μm) were adsorbed by the slag, and both the total oxygen content and inclusion density decreased during the LF refining process. After the Ti addition, the spherical inclusions changed into multilayer $CaO–Al_2O_3–MgO–TiO_x$ inclusions.

Ti is a highly active element and rapidly oxidizes at steelmaking temperatures. Therefore, to optimize the refining process, the addition of Ti should be reduced because of its high cost and undesirable oxidation. Herein, a large difference existed in the total oxygen content, Ti yield, and composition of the inclusions of Heat-1 and Heat-2 samples after the Ti addition during the LF refining. Therefore, the utilization of different refining slags significantly affected the oxygen content, Ti yield, and inclusions during the LF refining process, as discussed in the following sections.

4.1 TiO_2 activity of different slags

The activity of various structural units in different slags was calculated by using the ion–molecule coexistence theory. The thermodynamic model, used to calculate the active mass concentrations of structural units or ion couples in $CaO–CaF_2–SiO_2–Al_2O_3–MgO–TiO_2–MnO–Cr_2O_3$ slags

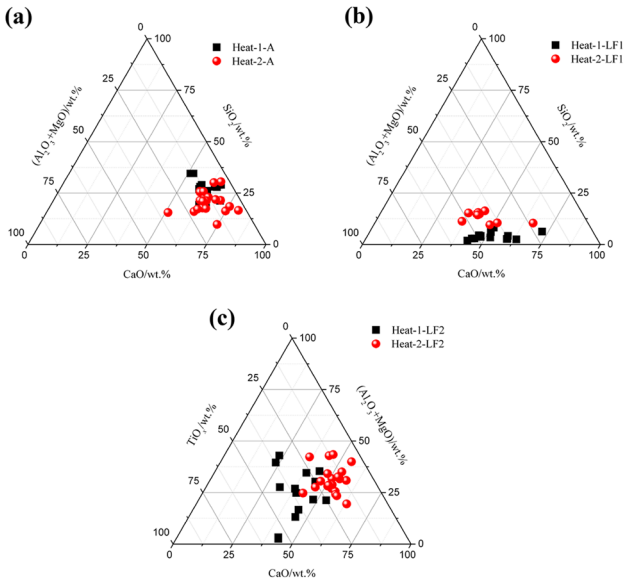

Fig. 6 Compositional distribution of inclusions at different stages of steelmaking process. **a** AOD; **b** LF1; **c** LF2

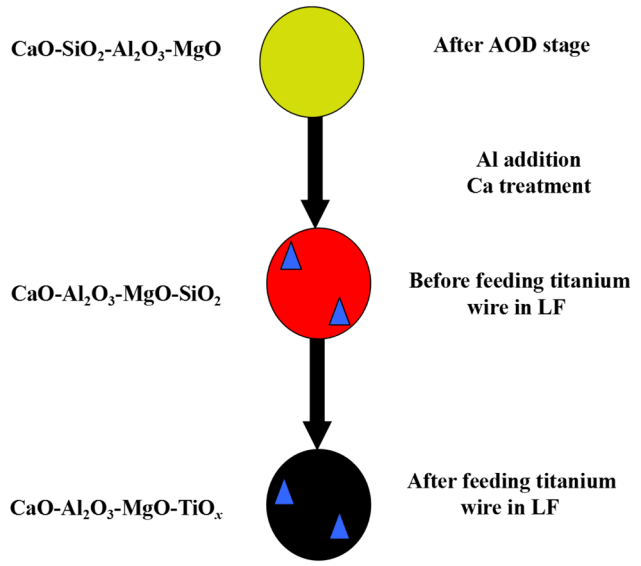

Fig. 8 Schematic illustration of formation mechanism of inclusions during 321 stainless steel refining process

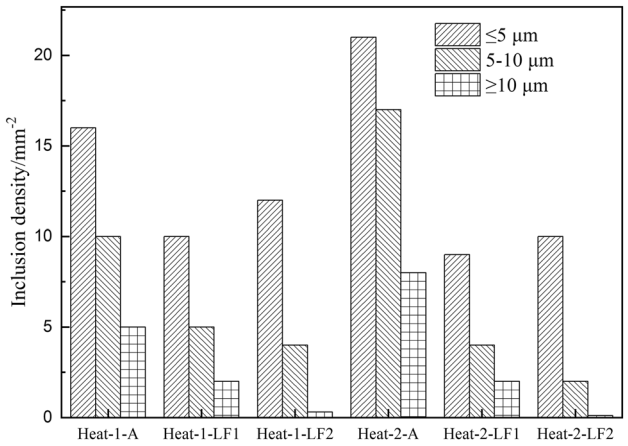

Fig. 7 Size distribution of inclusions at different stages of steelmaking process

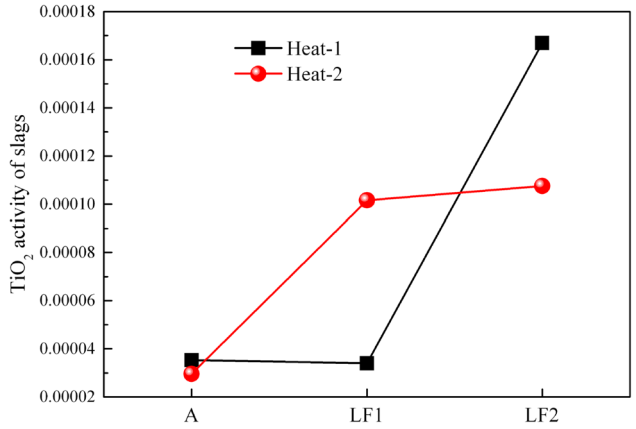

Fig. 9 TiO_2 activity of Heat-1 and Heat-2 samples at different stages of steelmaking process

equilibrated with the molten steel, is based on the assumptions referring to Refs. [19, 20].

In addition to the five simple ions, i.e., Ca^{2+}, Mg^{2+}, Mn^{2+}, F^{-}, and O^{2-}, and four simple molecules, i.e., SiO_2, TiO_2, Al_2O_3, and Cr_2O_3, several complex molecules also exist in $CaO–CaF_2–SiO_2–Al_2O_3–MgO–TiO_2–MnO–Cr_2O_3$ slag. Approximately, 34 different complex molecules were formed in the studied slags. The details of the calculation process are described elsewhere [19, 20].

The TiO_2 activity of different slags in Heat-1 and Heat-2 samples at different stages was calculated by using MATLAB 7.0 software, and the results are shown in Fig. 9. After the AOD process, the TiO_2 activity of different slags in Heat-1 and Heat-2 samples remained the same. In Heat-1 sample, which utilizing the conventional $CaO-Al_2O_3$-based slag, TiO_2 activity exhibited a small change from A to LF1. However, TiO_2 activity significantly increased after the Ti addition. In Heat-2 sample, using TiO_2-rich $CaO–Al_2O_3$-based slag, TiO_2 activity changed significantly. For instance, the TiO_2 activity of slag increased from 0.00003 to 0.00010 from A to LF1 stage, and then attained a stable value. Qian et al. [13] reported that the rate-determining step of Ti oxidation during steelmaking is the mass transfer on the slag side, and the oxidation of Ti exhibits an opposite trend to the activity of TiO_2. In the case of Heat-2 sample, TiO_2 activity of slag increased before the Ti addition and can suppress reactions (1) and (2). Hence, the TiO_2 content changed from

3.05 to 3.29 wt.%. During the LF refining process, the TiO_2 activity of slag in Heat-1 sample is 0.00003, indicating that Ti was rapidly oxidized and entered into the slag after the Ti addition.

$$2(Al_2O_3) + 3\,[Ti] = 3(TiO_2) + 4\,[Al] \quad (1)$$

$$(SiO_2) + [Ti] = (TiO_2) + [Si]. \quad (2)$$

4.2 Effect of refining slags on equilibrium oxygen content based on IMCT

Herein, 321 stainless steel is deoxidized with aluminum, and the chemical reaction in liquid steel is given as:

$$Al_2O_3 = 2[Al] + 3[O] \quad (3)$$

$$\lg K = \lg \frac{a_{Al}^2 \cdot a_O^3}{a_{Al_2O_3}} = -\frac{45,300}{T} + 11.62 \quad (4)$$

$$\lg a_O = \frac{-\frac{45,300}{T} + 11.62 + \lg a_{Al_2O_3} - 2\lg a_{Al}}{3} \quad (5)$$

where K refers to the distribution coefficient of each element; T represents the temperature; and a_i corresponds to the activity of each element i. The equilibrium oxygen content of Heat-1 and Heat-2 samples at different stages of the steelmaking process is calculated, and the results are shown in Fig. 10. The change in the equilibrium oxygen content in both the samples remained similar. The equilibrium oxygen content significantly decreased from A to LF1 and then slightly increased after the Ti addition during the LF refining process. Moreover, Heat-2 exhibited lower equilibrium oxygen content than Heat-1 before the Ti addition.

One should note that the lower oxygen content at equilibrium can suppress reaction (6) in the forward direction. Hence, the TiO_x and TiO_x-containing composite inclusions significantly reduced because of the reaction between Ti and O.

$$[Ti] + x[O] = (TiO_x). \quad (6)$$

4.3 Thermodynamic analysis of formation of CaO–Al_2O_3–MgO–TiO_x inclusions

The CaO–Al_2O_3–MgO–TiO_x inclusions were formed after the addition of Ti feeding wire into 321 molten steel during the LF refining process, as shown in Figs. 4 and 5. In order to study the formation mechanism of CaO–Al_2O_3–MgO–TiO_x complex inclusions, oxide stability diagram of the Al–Ti–O system, with iso-oxygen contours, in 321 stainless steel system at 1873 K was calculated by using FactSage™7.2 software, as shown in Fig. 11. The oxide stability diagram, as shown in Fig. 11, mainly consists of four regions: slag-liquid, Ti_2O_3, Ti_3O_5, and Al_2O_3. Moreover, the contents of Al and Ti in both Heat-1 and Heat-2 samples are marked in Fig. 11. In addition, Fig. 11 shows that the point of both Heat-1 and Heat-2 samples is located near the Al_2O_3–TiO_x zone. The collision of CaO–Al_2O_3–MgO liquid inclusions and TiO_x inclusions modified the CaO–Al_2O_3–MgO–TiO_x inclusions. In addition, the lower equilibrium oxygen content can suppress the reaction between Ti and O. Notably, the Heat-1 sample is located in the Ti_2O_3 zone, whereas Heat-2 sample is located in the Ti_3O_5 zone, indicating that

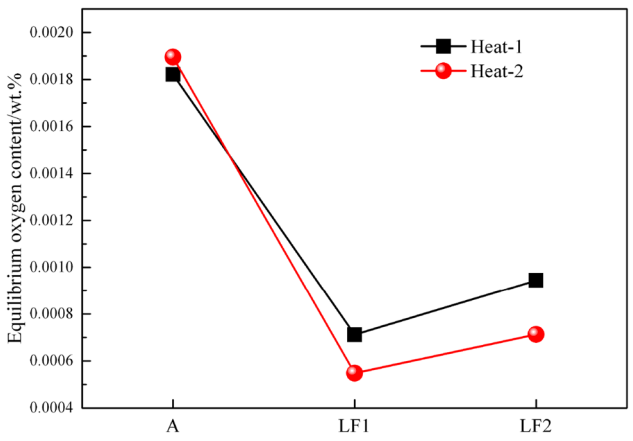

Fig. 10 Equilibrium oxygen content of Heat-1 and Heat-2 samples at different stages of steelmaking process

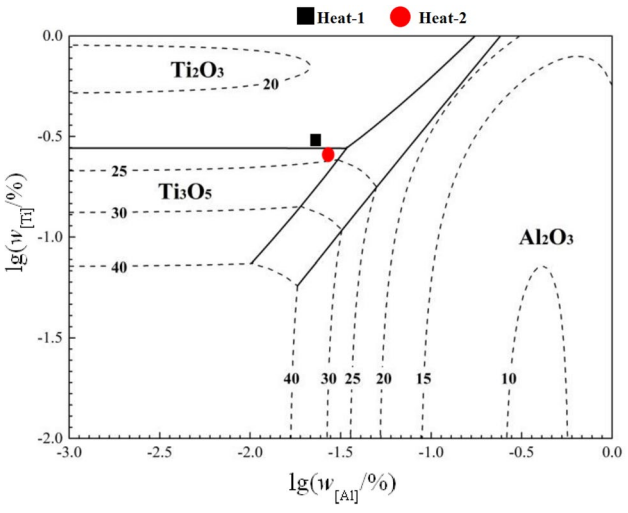

Fig. 11 Calculated oxide stability diagram of Al–Ti–O system, with iso-oxygen contours, in 321 stainless steel system at 1873 K

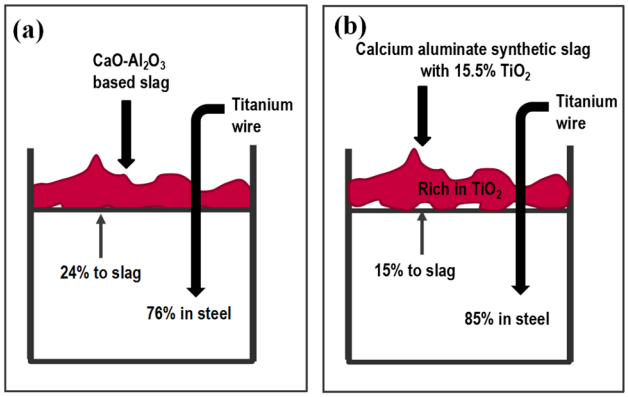

Fig. 12 Schematic illustration of influence of different refining slags on titanium yield during LF refining process in 321 stainless steel

a large quantity of Ti is oxidized during the formation of TiO_x inclusions in Heat-1 sample. These results are consistent with the composition distribution of the inclusions, as shown in Fig. 6.

Based on the experimental and thermodynamic analysis, the effect of different refining slags on the Ti yield during the LF refining is schematically illustrated in Fig. 12. In general, reactions (1), (2) and (6) occurred after the addition of Ti feeding wire into the molten steel. Then, the oxidation of Ti in the $CaO–Al_2O_3$ slag afforded 76% Ti yield. However, the Ti yield increased to 85% by using TiO_2-rich $CaO–Al_2O_3$ slag.

Furthermore, the thermodynamic calculations indicate that TiO_2 activity of the slag increased before the feeding of Ti wire into the molten steel. However, the oxidation of Ti in the slag exhibited an opposite trend to that of the TiO_2 activity, suppressing reactions (1), (2) and (6) in the forward direction. In contrast, the oxygen content decreased by using TiO_2-rich $CaO–Al_2O_3$ slag. Therefore, the content of TiO_x and TiO_x-containing composite inclusions, originating from the reactions between Ti and O, significantly reduced. Hence, Heat-2 sample exhibited a lower TiO_x content in $CaO–Al_2O_3–MgO–TiO_x$ inclusions than Heat-1 sample.

5 Conclusions

1. The total oxygen content and inclusion density decreased during the 321 steelmaking processes. The TO content and the Ti yield during the LF refining process can be controlled by using TiO_2-rich $CaO–Al_2O_3$-based slag.
2. The spherical $CaO–SiO_2–Al_2O_3–MgO$ inclusions existed in the 321 steel after the AOD process. Before the Ti addition in the LF process, the spherical $CaO–Al_2O_3–MgO–SiO_2$ inclusions were observed. After the Ti addition in the LF process, the inclusions changed to multilayer $CaO–Al_2O_3–MgO–TiO_x$ inclusions. Moreover, the inclusion density and TiO_x content of $CaO–Al_2O_3–MgO–TiO_x$ inclusions of Heat-2 sample, utilizing TiO_2-rich $CaO–Al_2O_3$-based slag, were lower than those of Heat-1 sample, using traditional $CaO–Al_2O_3$-based slag.
3. When TiO_2-rich $CaO–Al_2O_3$-based slag was used, the TiO_2 activity of the slag increased, and the equilibrium oxygen content significantly decreased from the AOD to the LF processes. The oxidation of Ti exhibited an opposite trend to that of the TiO_2 activity in the slag. The lower equilibrium oxygen content suppressed the reactions between Ti and O.

Acknowledgements The authors gratefully acknowledge the support of the National Natural Science Foundation of China (Grant No. 51374020), the State Key Laboratory of Advanced Metallurgy at the University of Science and Technology Beijing (USTB), and the Jiuquan Iron and Steel Group Corporation.

References

[1] G.V. Prasad Reddy, P.M. Dinesh, R. Sandhya, K. Laha, T. Jayakumar, Int. J. Fatigue 92 (2016) 272–280.
[2] M. Haj, H. Mansouri, R. Vafaei, G. R. Ebrahimi, A. Kanani, Int. J. Miner. Metall. Mater. 20 (2013) 529–534.
[3] H.Y. Luo, Y.B. Zhang, H.D. Li, J.L. Lv, Y. Ma, J. Alloy. Compd. 696 (2017) 1235–1243.
[4] M.W. Spindler, G. Knowles, S. Jacques, C. Austin, Mater. High Temp. 31 (2014) 284–304.
[5] P. Huilgol, K.R. Udupa, K.U. Bhat, Int. J. Miner. Metall. Mater. 25 (2018) 190–198.
[6] J.H. Park, S.B. Lee, H.R. Gaye, Metall. Mater. Trans. B 39 (2008) 853–861.
[7] J.Y. Li, G.G. Cheng, Q. Ruan, J.X. Pan, X.R. Chen, ISIJ Int. 58 (2018) 1042–1051.
[8] H.G. Zheng, W.Q. Chen, Q. Liu, P.F. Duan, L.R. Zhao, H.L. Wang, J. Iron Steel Res. 17 (2005) No. 1, 14–18.
[9] Q. Ruan, G.Y. Qian, J.X. Pan, X.R. Chen, G.G. Cheng, Steelmaking 32 (2016) No. 4, 39–43.
[10] H.G. Zheng, W.Q. Chen, S.M. Bo, M.S. Liu, Iron and Steel 40 (2005) No. 5, 21–24.
[11] J.Y. Li, G.G. Cheng, Q. Ruan, J.X. Pan, X.R. Chen, Metall. Mater. Trans. B 49 (2018) 2357–2369.
[12] X. Yin, Y.H. Sun, Y.D. Yang, X.F. Bai, M. Barati, A. Mclean, Metall. Mater. Trans. B 47 (2016) 3274–3284.
[13] G.Y. Qian, F. Jiang, G.G. Cheng, C.S. Wang, Metall. Res. Technol. 111 (2014) 229–231.
[14] K. Choi, Y. Kang, I. Sohn, Metall. Mater. Trans. B 47 (2016) 1520–1525.
[15] J.Y. Yu, Y. Kang, I. Sohn, Metall. Mater. Trans. B 45 (2014) 113–122.
[16] H.G. Zheng, W.Q. Chen, J. Univ. Sci. Technol. Beijing 13 (2006) 16–20.
[17] C.W. Seo, S.H. Kim, S.K. Jo, M.O. Suk, S.M. Byun, Metall. Mater. Trans. B 41 (2010) 790–797.
[18] R. Lencina, A. Malfliet, B. Touzo, M.X. Guo, AISTech 2018 (2018) 1343–1350.
[19] X.M. Yang, C.B. Shi, M. Zhang, G.M. Chai, F. Wang, Metall. Mater. Trans. B 42 (2011) 1150–1180.
[20] X.M. Yang, M. Zhang, C.B. Shi, G.M. Chai, J. Zhang, Metall. Mater. Trans. B 43 (2012) 241–266.